A micro-mechanically based continuum damage model for fatigue life prediction of filled rubbers

Julie Grandcoin, Adnane Boukamel, Stéphane Lejeunes

A micro-mechanically based continuum damage model for fatigue life prediction of filled rubbers

J. Grandcoin[a], A. Boukamel[b], S. Lejeunes[a,*]

[a] *LMA, CNRS, UPR 7051, Aix-Marseille Univ, Centrale Marseille, F-13402 Marseille Cedex 20, France*
[b] *Ecole Hassania des Travaux Publics, KM 7, Route d'El Jadida, B.P 8108, Oasis, Casablanca, Maroc*

Abstract

This paper presents a continuum damage model based on two mechanisms: decohesion between fillers and matrix at a micro-scale followed by a crack nucleation at a macro-scale. That scenario was developed considering SEM observations and an original experimental procedure based on simple shear and tension specimens. Damage accumulation is related to fatigue life using the continuum damage mechanics (CDM). The material behavior is investigated using the statistical framework introduced by Martinez et al. (2011). A Finite Element implementation is proposed and some numerical examples are provided.

Key words: Fatigue, Damage, Rubber, Finite Element

1. Introduction

Elastomeric materials are widely used by many industries: automotive, aeronautic... In many applications, elastomeric parts are closely linked to security and require specific qualification tests which impact product costs and safety of end-users. Therefore a perfect knowledge of the mechanical behavior and robust constitutive models are needed. Modern elastomeric components are composed of more and more complex rubber systems including different fillers and rubber bases (natural or synthetic or both). In many applications, these materials are subjected to cyclic loadings and are designed to damp energy. For these materials, it is mainly observed a damage initiation at a micro level by filler/matrix decohesion or by cavitation growth inside matrix. These phenomena give rise to a propagation at a macro level by the help of coalescence of voids or by crack propagation leading at the end to the failure of part. Identifying the physical phenomenon that takes place during high cycle fatigue test is a very hard task because multi-physics and multi-scale effects are occurring. For instance, temperature, crystallization, stress triaxiality, stress ratio, hydrostatic pressure, chemical aging are playing important roles on fatigue.

In the literature, one can distinguish at least three approach to model the damage due to cyclic loadings for rubber materials:

- The first one relates to prediction of crack growth. These approaches often assume that initial defects are pre-existing in the material but no information on defects localization or size is required. Starting from experimental curves that plot the value of a predicting quantity upon the log of number of cycles (so called Whöler curves or Haigh's diagrams) many predictor or criteria have been proposed. These criteria can be based on a mechanical quantity that is not directly related to local mechanisms caused by damage: maximum principal strain (e.g. Cadwell et al. (1940)), strain energy density (e.g. Beatty (1964)), strain based phenomenological model (e.g. Robisson (2000)), stress based with Dang Van

*Corresponding author
Email addresses: boukamel@ehtp.ac.ma, tel: 0212520420512 (A. Boukamel), lejeunes@lma.cnrs-mrs.fr, tel: 033491054382,fax: 033491054749 (S. Lejeunes)

sphere (e.g. Brunac et al. (2009)), dissipated energy density (e.g. Lacroix et al. (2005); Poisson et al. (2011)). Other approaches try to embed more information on real local-mechanisms or idealized ones. Saintier et al. (2006) have proposed a multi-axial criteria based on principal stresses with a reinforcing term linked to crystallization. In Mars (2002) a new criteria has been introduced, an incremental strain energy, which is defined on an unknown material plane that represents the cracking plane, is computed (see also Zine et al. (2011)). Verron et al. (2005) have proposed a promising approach using a criteria based on the Eshelby tensor (configurational mechanics). This criteria shows very interesting results in multi-axial conditions (see also Verron and Andriyana (2008); Andriyana et al. (2002)). Interesting comparisons of criteria can be found in Poisson et al. (2011) for a polychloroprene rubber in multi-axial conditions and in Previati and Kaliske (2012) for an application on truck tires. A more complete review of criteria can be found in Mars (2001); Mars and Fatemi (2002).

- The second one, consists on using fracture mechanics to predict crack initiation and propagation. One can find, for instance, power laws that describe the evolution of the crack length upon cycles as a power function of the energy release rate, see Lake and Lindley (1965) for experimental results. Fracture mechanics based models require a knowledge of initial defects which is very restrictive for rubber because these defects are very difficult to identify.

- The last approach is based on continuum damage mechanics (CDM) and consists in the introduction of, at least, one internal variable in the material behavior that represents the normalized quantity of damage (cracks, voids, etc) in the material. This approach has been firstly used for elastomeric materials to described short time history effect like the Mullins effect (see Chagnon et al. (2004)). For high cycle fatigue, the ideas of Lemaitre (1985) can be applied to rubber. A cumulative rule for damage is assumed (e.g. linear) and the damage evolution is integrated cycle by cycle. Therefore, the damage evolution can be directly related to the number of cycles. This approach has been used in Wang et al. (2002); Ayoub et al. (2011, 2012). To the authors knowledge only hyperelasticity has been considered in previous works, however the mechanical dissipation plays a fundamental role on the fatigue life in rubber materials.

In the present work a silicone rubber filled with silica is considered. This material is used in aeronautic structures to damp a mechanical energy due to vibrations. In industrial applications, rubber is mainly loaded in simple shear and the prediction of a stiffness loss is critical for the safety of the structure. It is proposed to use the CDM approach to predict this stiffness loss and the fatigue life. Starting from micro-mechanical observations and from an original experimental campaign of fatigue tests on simple shear and tension specimens, we propose a two scale model: the first scale aims at representing the voids or cracks initiation near the agglomerate of fillers and the second scale represents the voids or cracks growth in the rubber matrix. The main originality of this paper is that the proposed driving force for damage is defined from a returnable energy rate which is integrated over a cycle. This energy represents the difference between the given energy and the dissipated one for a stabilized cycle. The effect of stress multi-axiality or the effect of the mean stress are embedded in this energetic damage rule.

The constitutive behavior developed in this paper is based on the statistical framework of Martinez et al. (2011). In this framework, the Cauchy stress is viewed as the sum of a matrix part (hyperelastic) and a continuous contribution due to agglomerates (visco-hyperelastic). A statistical variable and a probability function are introduced to represent a continuous number of relaxation mechanisms. The statistical variable is related to the activation energy of each dissipation mechanisms (related to each population of agglomerates). The main advantage of this approach lies in its ability to cover a large range of strain rates and amplitudes with a small number of material parameters. The connection between the damage model and the constitutive model is straight-forward, the micro scale of damage is taken into account in the probability function as damage in agglomerates tends to decrease the relaxation mechanisms. The macro scale is classically related to the cracks grow in the matrix.

A classical variational formalism is adopted and a finite element implementation is derived. The mechanical flow rules are integrated following the proposal of Lejeunes et al. (2011). Damage is only post-treated by computing the returnable energy rate over one stabilized cycle.

The paper is organized as follows. In a first part, the micro-mechanical observations and the main results of the experimental characterization are presented and discussed. In a second part, a new statistical constitutive model is introduced to represent the mechanical behavior. The CDM approach is then detailed in a third section. The finite elements implementation is briefly exposed and some numerical results are shown in the last section.

2. Experimental results

2.1. micro-mechanical observations

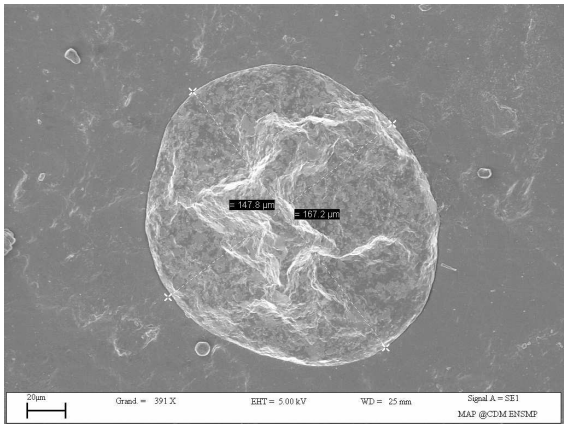

(a) Virgin material (large agglomerate of silica)

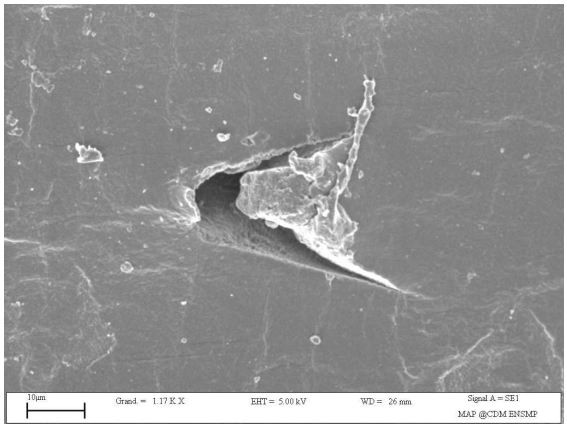

(b) After fatigue: void near a filler (probably due to matrix/filler decohesion)

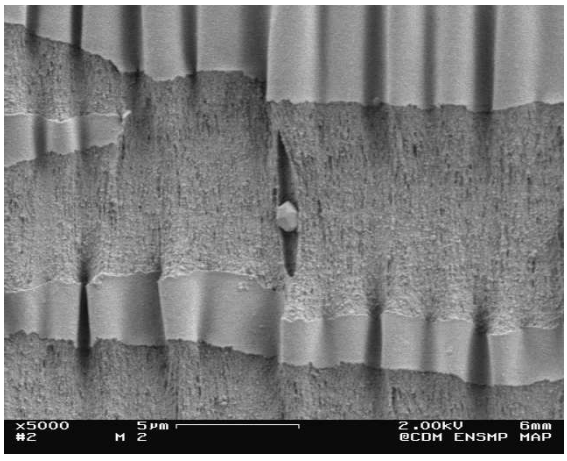

(c) After fatigue: micro-crack normal to the load direction

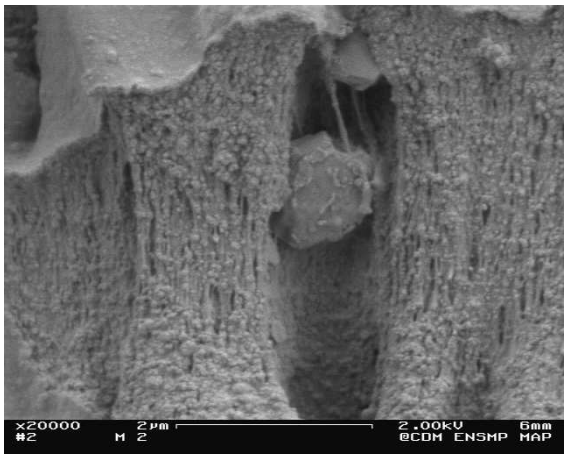

(d) After fatigue: zoom on micro-crack with ligaments between filler and matrix.

Figure 1: SEM observations of Silica agglomerates in a silicone rubber.

To identify micro-mechanisms that take place during cyclic fatigue test, we made some SEM observations at the "Centre des Materiaux" of the "Ecoles des Mines de Paris". Figure 1(a) shows a large agglomerate of

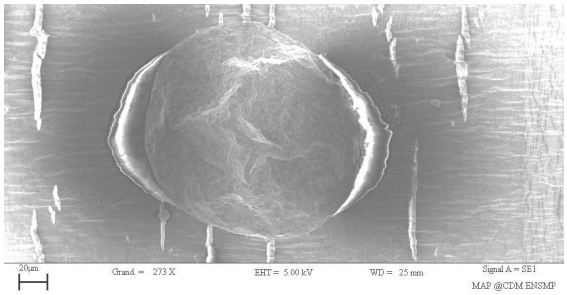

(a) matrix/filler decohesion at 100% of uniaxial-tension: the tension direction is in the same direction as the one of loading (horizontal direction for this image)

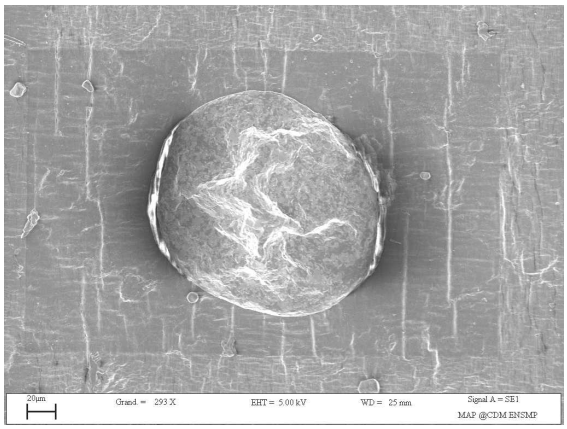

(b) matrix/filler decohesion at 0% of uniaxial-tension: cavitation at the poles of the agglomerate

Figure 2: SEM observations of silica agglomerates in a silicone rubber after fatigue: In-Situ tension test. Due to the metalic agent to deposit on the surface of the specimen prior to In-Situ testing, the cracks observed can not be directly related to the rubber matrix.

silica inside the matrix for a virgin sample, at this scale ($20\mu m$) the matrix is dense, no voids are observed. The figure 1(b) shows a smaller agglomerate for a sample which has been cut inside a uni-axial tension specimen. This specimen has been previously submitted to 100000 cycles of fatigue (frequency is 1Hz and the strain amplitude is $150\% \pm 50\%$). A decohesion of the filler-matrix interface can be observed. On figure 1(c) and 1(d), one can observed the initiation of a micro-crack (5 μm length on figure 1(c)) which is normal to the direction of the fatigue loading. This micro-crack contains a filler at its center and it seem quite natural to postulate that the filler can be viewed as a defect that originated the crack, however we have no proof that the crack was not previously here.
The SEM also provide the availability to do In-situ observations (while applying a mechanical loading). Figures 2 show a result of such an experiment. The micro sample, which has been cut in a previously fatigued specimen, is submitted to an uni-axial tension test (the loading direction is as the one of fatigue). A filler/matrix decohesion is seen, in the same direction as the one of loading. When the load is released a void remains at the poles of the agglomerate (even after a long time to eliminate viscous effects).

From these observations we can conclude that filler/matrix interaction plays a fundamental role on the fatigue behavior at the micro-scale for this material. Decohesion seems to be the principal micro-mechanism that can lead to the formation of micro-cracks. For uni-axial loading and for a non-cristallizable matrix, these micro-cracks propagate in the matrix in a direction which is normal to the load direction without bifurcations. Furthermore, this decohesion phenomena leads to a volume variation because voids remain in the unloading state. However, transposing these results at the macro-scale is not obvious. Therefore we prefer to neglect it in the following as we believe that at the macro-scale damage due to fatigue is affecting more the deviatoric part than the spherical one. To the authors opinion the investigation of volume variation is a very hard topic as concurrent phenomena are taking place in rubber that affect the volume variation: cavitation, crystallization, network reorganization or stress softening, thermal dilatation, etc.

2.2. fatigue characterization

The aim of the experimental campaign is to characterize the mechanical behavior after a given number of cycles. Usually, damage is characterized through a loss of rigidity. However, rubber materials exhibit other softening effects like the Mullins effect or thermal softening induced by self-heating for high dissipative materials.

In fact, the increase of temperature during the fatigue test implies a softening of the material. If the

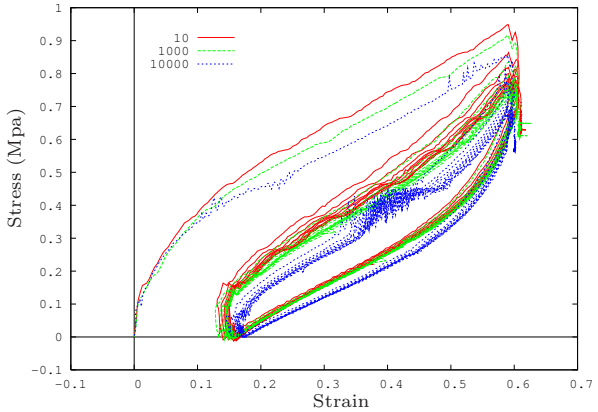

(a) Triangular cyclic tension tests after N cycles of fatigue (the fatigue configuration is 0.5Hz and 150% of mean strain and ±150% of dynamic strain).

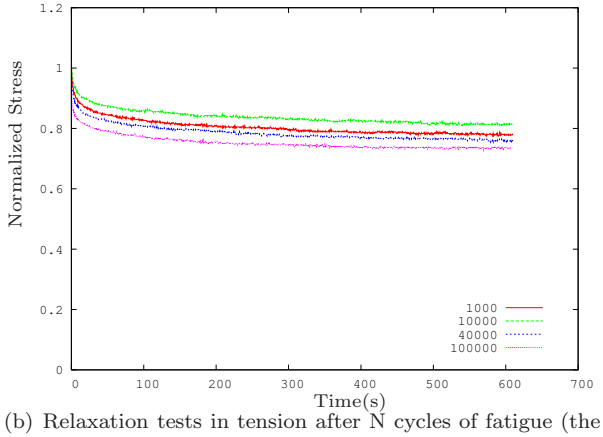

(b) Relaxation tests in tension after N cycles of fatigue (the fatigue configuration is 0.5Hz and 25% of mean strain and ±25% of dynamic strain).

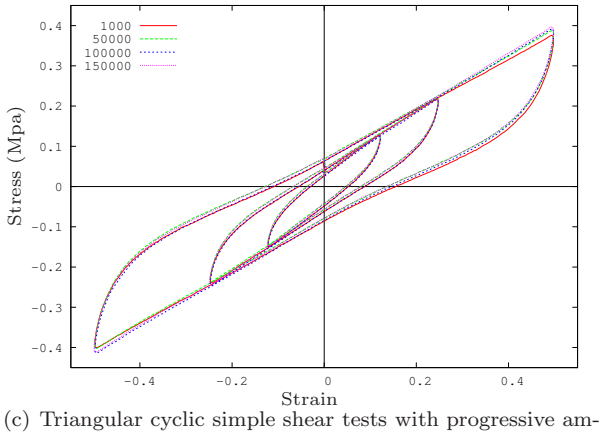

(c) Triangular cyclic simple shear tests with progressive amplitude, after N cycles of fatigue (the fatigue configuration is 15Hz and 12.5% of mean strain and ±25% of dynamic strain).

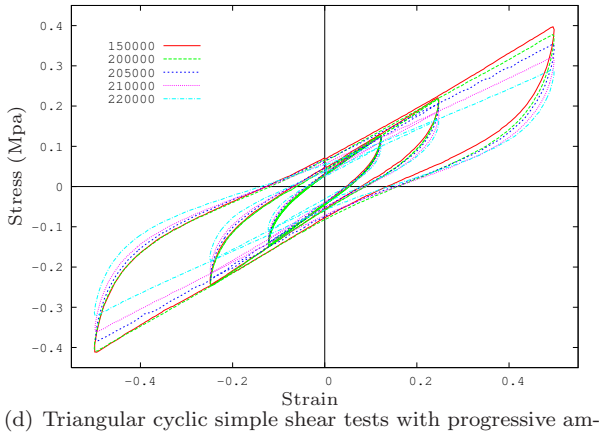

(d) Triangular cyclic simple shear tests with progressive amplitude, after N cycles of fatigue (the fatigue configuration is 15Hz and 12.5% of mean strain and ±25% of dynamic strain).

Figure 3: Typical results obtained from the characterization tests after fatigue (step 4 of the experimental campaign)

acquisitions are done during fatigue tests, the thermal softening can hide the damage effect which also leads to a softening. To clearly identify the evolution of damage with a remove of the thermal and the Mullins softening, we have defined an original experimental protocol. The characterization of the behavior at a given number of fatigue cycles N requires the following steps:

1. 20 cycles at a strain amplitude 10% higher than the maximum strain amplitude during fatigue to remove Mullins effect,
2. N fatigue cycles with a regulated temperature (only the ambient temperature inside the climatic chamber is controlled),
3. two rest days (the sample is stress free) to remove thermal and long time viscous effects,
4. mechanical characterization with: (i) a quasi-static test, (ii) triangular cyclic tests at various strain rates and various strain amplitudes and (iii) relaxation tests.

All these tests have been performed on a hydraulic machine which can be equipped with an adiabatic chamber in which internal temperature can be regulated. For shear specimens, displacement is controlled and load is recorded. For tension specimen depending on the load case, the control can be done on displacement or on load for the unloading phase. Therefore it can be avoided buckling due to relaxation. The signal is

sinusoidal. In the following, for each fatigue test it is provided the frequency of the signal, the maximum strain amplitude, and the mean strain if it is not zero. Tension specimens are dumbbell shaped of type H2 with a square rectangular cross-section of 5x2 mm^2. For shear tests, it is used specific double shear specimens. These specimen are composed of two blocks of rubber with a central rigid aluminum layer and two external rigid aluminum layers. The rubber blocks are 96 mm long, 5 mm high and 20 mm large. Furthermore the end sections have a meniscus shape to ensure that cracks do not initiate at the interface aluminum/rubber. Each specimen is submitted further time to the steps 1 to 4 with increasing value of N (typically N=1000, 10000, 100000,...)

The previous procedure is time consuming and only a repeatability of two was achieved for simple shear specimens and three for tension specimens. Figures 3, show an example of experimental results obtained from the step 4 (characterization tests). In figure 3(a) and 3(d) we clearly see a loss of stiffness and a decrease of the dissipated energy when N (the number of fatigue cycles) increases. More surprisingly, we often observe during the first cycles of fatigue in simple shear tests an increase of the stiffness (see figure 3(b) and 3(c)) previously to damage phenomena. This observation will be discussed below.

To proceed further, it is defined global characteristics (stiffness and dissipation) from the figure 4. Figures 5 and 6 show a comparison of different fatigue configurations with tension and simple shear specimens. Each point is obtained by following all the steps previously described. For each quasi-static characterization tests after fatigue, we determine a global stiffness and a global dissipation on a stabilized cycle. The stiffness and the dissipation values are normalized and it is observed the following behavior: in a first step the global stiffness and the dissipation are increasing followed by a second step in which both stiffness and dissipation are rapidly decreasing. Furthermore this effect is more pronounced for shear specimens. We propose the following scenario to explain these observations:

Step 1 During the first cycles, fillers-matrix bonds begin to break and the filler-matrix decohesion is starting. In the meantime, new chemical bonds are formed in the matrix due to the thermal aging that results from the self-heating of the material. These effects are in competition but thermal aging takes the lead and a global stiffening is observed.

Step 2 For a large number of cycles, damage is growing and propagates to the matrix. Thermal aging is less sensitive due to the stabilization of the self-heating phenomena. A global decrease of the stiffness is observed.

The previous scenario also furnishes an explanation to the fact that shear specimens are more sensitive to thermal aging: in simple shear damage is more localized and less homogeneous than for tension and self-heating phenomena is stronger.

Due to the competition between damage and thermal aging it is a very hard task to determine when initiation of damage in the matrix takes place. To proceed further we propose to consider the intersection of the two curves as an important characteristic number of cycles for which it can be clearly said that the mechanical behavior is affected by damage. Different fatigue configurations are summed up in the table 1. The loss of stiffness (and dissipation) is strongly dependent on the strain amplitude and it seems also sensitive to the mean strain: increasing R-ratio leads to higher number of cycles. This effect may be related to previous works: e.g. Legorju-jago and Bathias (2002); Saintier et al. (2011) show that life-time increases for positive R-ratio on diabolo specimens. They show that cristallization plays an important role on it but Poisson et al. (2011) also observed it for non-cristallizable rubber. Frequency does not seems to play a major role but more tests are needed to study this effect.

	Maximum strain amplitude (with zero mean strain)			Maximum strain amplitude (with 12.5% of mean strain)		
	$12,5\%$	25%	50%	$12,5\%$	25%	50%
6Hz	> 1000000	168000	30000	> 1000000	190000	$[30000, 50000]$
15Hz	> 1000000	148000	30000	> 1000000	191000	$[30000, 50000]$

Table 1: Number of cycles for which global stiffness and global dissipation start to decrease for the simple shear fatigue test

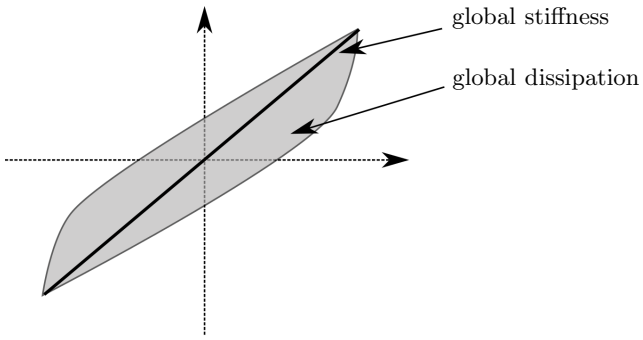

Figure 4: Global characteristics: global stiffness (slope of the secant of the hysteresis) and global dissipation (area of the hysteresis)

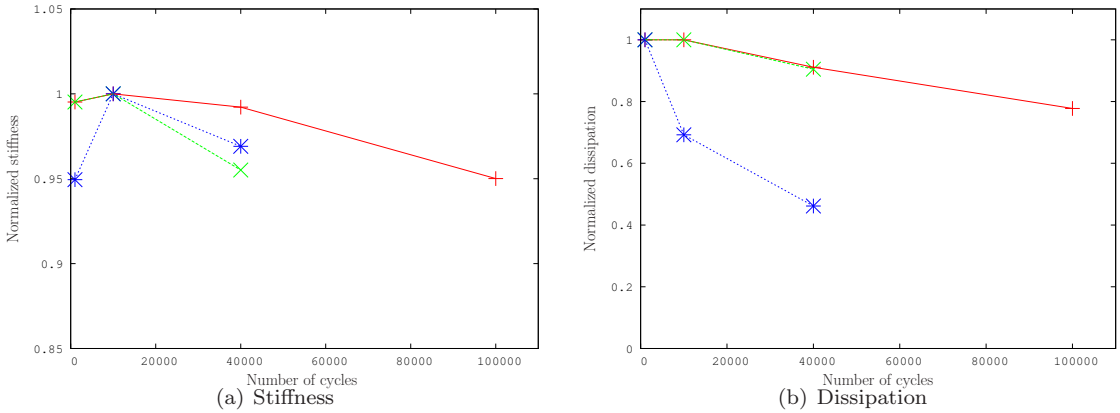

(a) Stiffness (b) Dissipation

Figure 5: Evolution of the global characteristics for quasi-static cyclic test in tension (+ : After fatigue at 10% of strain amplitude, × :After fatigue at 15% of strain amplitude et ∗ : After fatigue at 30% of strain amplitude)

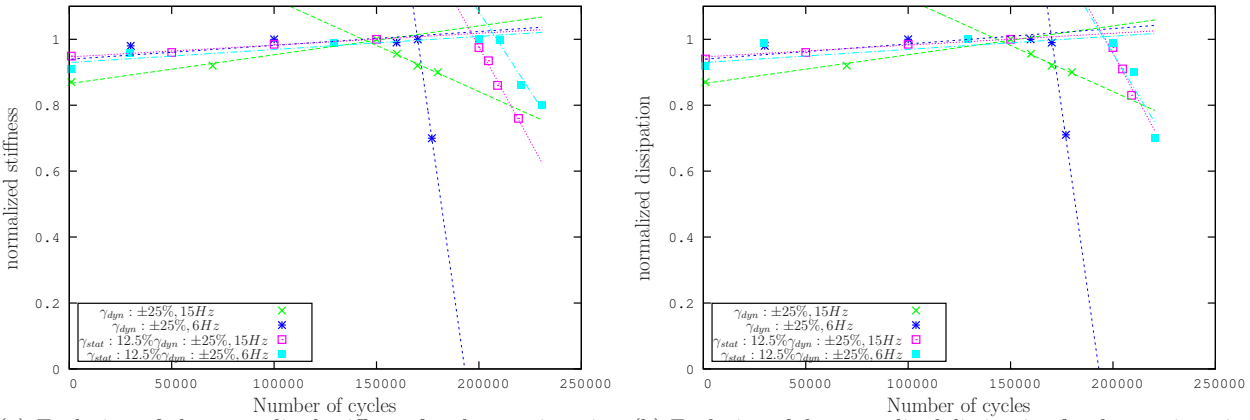

(a) Evolution of the normalized stiffness for the quasi-static cyclic test after fatigue

(b) Evolution of the normalized dissipation for the quasi-static cyclic test after fatigue

Figure 6: Global characteristics of the mechanical response upon fatigue for simple shear specimens.

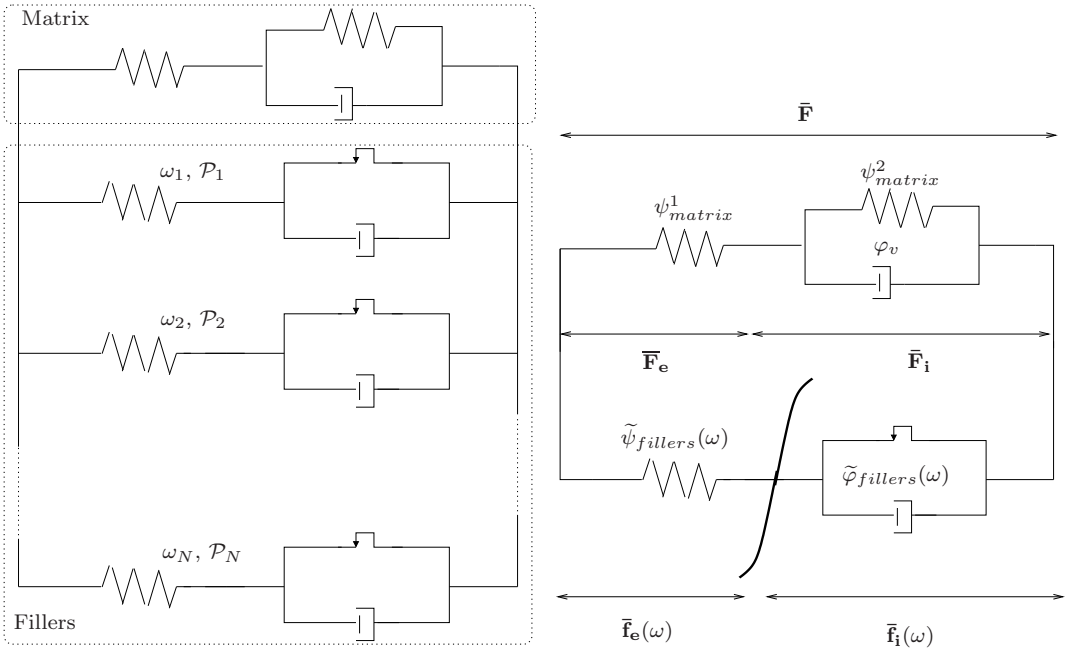

(a) Generalized model (b) Statistical model

Figure 7: Mechanical constitutive model

3. Constitutive model

3.1. Mechanical behavior

In this paper, we extend a previously developed approach for the modeling of the dynamical behavior of filled rubbers (see Martinez et al. (2011)). This approach is micro-mechanically motivated and is based on a statistical representation of agglomerates and aggregates of fillers. Each population of aggregate or agglomerate is associated to a couple of thermodynamical potentials: a specific free energy and a pseudo-potential of dissipation. A random variable ω, is introduced and relates to the energy of activation of a micro-mechanism of relaxation. It is also introduced $P(\omega)$, a probability density function that describes the range of energies of activation that is covered by the material. Therefore it is possible to take into account of a large number of relaxation mechanisms without increasing the number of material parameters.

It is assumed that the global deformation of the matrix and of a representative volume element of filler aggregates[1] are the same (affine model). The global framework can be summarized by the figure 7. In this work, the matrix is described by a visco-elastic model of Poynting-Thomson. This viscosity is introduced to represent long time effects. Each population of agglomerate is described by an elasto-visco-plastic model. Following Flory (Flory (1961)), the deformation gradient $\mathbf{F}$ is split into an isochoric part: $\bar{\mathbf{F}}$ and a volumetric part: $J^{1/3}\mathbf{1}$, where $J = \det \mathbf{F}$ and $\mathbf{1}$ stands for the identity tensor (Cartesian metric is used). As no viscous effects are generally observed for volumetric deformation in rubber, the isochoric deformation gradient is split as follows:

$$\bar{\mathbf{F}} = \overline{\mathbf{F}}_\mathbf{e}\bar{\mathbf{F}}_\mathbf{i} = \bar{\mathbf{f}}_\mathbf{e}(\omega)\bar{\mathbf{f}}_\mathbf{i}(\omega) \tag{1}$$

where $\overline{\mathbf{F}}_\mathbf{e}$ and $\bar{\mathbf{F}}_\mathbf{i}$ are elastic and inelastic isochoric deformation gradients in the matrix and $\bar{\mathbf{f}}_\mathbf{e}(\omega)$ and $\bar{\mathbf{f}}_\mathbf{i}(\omega)$ are elastic and inelastic isochoric deformation gradient in the agglomerates. The themodynamical potentials

[1] the RVE of aggregates is assumed to be composed of fillers and gum (occluded gum and bound rubber).

(free energy and pseudo potential of dissipation) are therefore functions of elastic and inelastic gradients but also depend on ω as follows:

$$\begin{cases} \psi = \psi_{matrix}(\bar{\mathbf{B}}_\mathbf{i}, \bar{\mathbf{B}}_\mathbf{e}) + \displaystyle\int_0^\infty \tilde{\psi}_{fillers}\left(\omega, \bar{\mathbf{b}}_\mathbf{e}(\omega)\right) P(\omega) d\omega + \psi_{vol}(J) \\ \varphi = \varphi_{matrix}(\bar{\mathbf{D}}_\mathbf{i}^\mathbf{o}) + \displaystyle\int_0^\infty \tilde{\varphi}_{fillers}\left(\omega, \bar{\mathbf{d}}_\mathbf{i}^\mathbf{o}(\omega)\right) P(\omega) d\omega \end{cases} \tag{2}$$

where $\bar{\mathbf{B}}_\mathbf{e} = \overline{\mathbf{F}}_\mathbf{e}\overline{\mathbf{F}}_\mathbf{e}^{\,T}$, $\bar{\mathbf{b}}_\mathbf{e}(\omega) = \bar{\mathbf{f}}_\mathbf{e}(\omega)\bar{\mathbf{f}}_\mathbf{e}(\omega)^T$, $\bar{\mathbf{B}}_\mathbf{i} = \bar{\mathbf{F}}_\mathbf{i}\bar{\mathbf{F}}_\mathbf{i}^T$ are elastic and inelastic left Cauchy-Green tensors, $\bar{\mathbf{D}}_\mathbf{i}^\mathbf{o}$ and $\bar{\mathbf{d}}_\mathbf{i}^\mathbf{o}(\omega)$ are objective rates of the inelastic deformations defined from:

$$\bar{\mathbf{D}}_\mathbf{i}^\mathbf{o} = \mathbf{R}_e\bar{\mathbf{D}}_\mathbf{i}\mathbf{R}_e{}^T = \frac{1}{2}\mathbf{R}_e(\dot{\bar{\mathbf{F}}}_\mathbf{i}\bar{\mathbf{F}}_\mathbf{i}^{-1} + \bar{\mathbf{F}}_\mathbf{i}^{-T}\dot{\bar{\mathbf{F}}}_\mathbf{i}^{\,T})\mathbf{R}_e{}^T \tag{3}$$

$$\bar{\mathbf{d}}_\mathbf{i}^\mathbf{o}(\omega) = \mathbf{r}_e(\omega)\bar{\mathbf{d}}_\mathbf{i}(\omega)\mathbf{r}_e{}^T(\omega) = \frac{1}{2}\mathbf{r}_e(\omega)(\dot{\bar{\mathbf{f}}}_\mathbf{i}(\omega)\bar{\mathbf{f}}_\mathbf{i}^{-1}(\omega) + \bar{\mathbf{f}}_\mathbf{i}^{-T}(\omega)\dot{\bar{\mathbf{f}}}_\mathbf{i}^{\,T}(\omega))\mathbf{r}_e{}^T(\omega) \tag{4}$$

where $\mathbf{R}_e$ and $\mathbf{r}_e(\omega)$ are coming from the polar decomposition of $\overline{\mathbf{F}}_\mathbf{e}$ and $\bar{\mathbf{f}}_\mathbf{e}(\omega)$.
Neglecting thermal effect, the dissipation inequality (or Clausius Duhem inequality) in eulerian configuration can be written as:

$$\phi = \boldsymbol{\sigma} : \mathbf{D} - \rho\dot{\psi} \geq 0 \tag{5}$$

The variation of the free energy, eq. (2), is given by:

$$\dot{\psi} = \frac{\partial\psi_{matrix}}{\partial\bar{\mathbf{B}}_\mathbf{e}} : \dot{\bar{\mathbf{B}}}_\mathbf{e} + \frac{\partial\psi_{matrix}}{\partial\bar{\mathbf{B}}_\mathbf{i}} : \dot{\bar{\mathbf{B}}}_\mathbf{i} + \int_0^\infty \frac{\partial\tilde{\psi}_{fillers}\left(\omega, \bar{\mathbf{b}}_\mathbf{e}(\omega)\right)}{\partial\bar{\mathbf{b}}_\mathbf{e}(\omega)} : \dot{\bar{\mathbf{b}}}_\mathbf{e}(\omega) P(\omega) d\omega + \frac{\partial\psi_{vol}}{\partial J}\dot{J} \tag{6}$$

The time variation of elastic and inelastic Cauchy Green tensors and of volume variation are given by:

$$\dot{J} = J\left(\mathbf{1} : \mathbf{D}\right) \tag{7}$$

$$\dot{\bar{\mathbf{B}}}_\mathbf{i} = \bar{\mathbf{L}}_\mathbf{i}\bar{\mathbf{B}}_\mathbf{i} + \bar{\mathbf{B}}_\mathbf{i}\bar{\mathbf{L}}_\mathbf{i}^\mathrm{T} \tag{8}$$

$$\dot{\bar{\mathbf{B}}}_\mathbf{e} = \mathbf{L}\bar{\mathbf{B}}_\mathbf{e} + \bar{\mathbf{B}}_\mathbf{e}\mathbf{L}^\mathrm{T} - 2\bar{\mathbf{V}}_\mathbf{e}\bar{\mathbf{D}}_\mathbf{i}^\mathbf{o}\bar{\mathbf{V}}_\mathbf{e} - \frac{2}{3}(\mathbf{1} : \mathbf{D})\bar{\mathbf{B}}_\mathbf{e} \tag{9}$$

$$\dot{\bar{\mathbf{b}}}_\mathbf{e}(\omega) = \mathbf{L}\bar{\mathbf{b}}_\mathbf{e}(\omega) + \bar{\mathbf{b}}_\mathbf{e}(\omega)\mathbf{L}^\mathrm{T} - 2\bar{\mathbf{v}}_\mathbf{e}(\omega)\bar{\mathbf{d}}_\mathbf{i}^\mathbf{o}(\omega)\bar{\mathbf{v}}_\mathbf{e}(\omega) - \frac{2}{3}(\mathbf{1} : \mathbf{D})\bar{\mathbf{b}}_\mathbf{e}(\omega) \tag{10}$$

where $\bar{\mathbf{V}}_\mathbf{e}$ and $\bar{\mathbf{v}}_\mathbf{e}(\omega)$ are the pure deformations coming from the polar decomposition of $\overline{\mathbf{F}}_\mathbf{e}$ and $\bar{\mathbf{f}}_\mathbf{e}(\omega)$. Using equations (10), (9), (8), (7) in (6) and reporting the result in (5), it is obtained the following expression of the dissipation:

$$\begin{aligned} \phi = &\left(\boldsymbol{\sigma} - \rho_0 J^{-1}\left(2\bar{\mathbf{B}}_\mathbf{e}\frac{\partial\psi_{matrix}}{\partial\bar{\mathbf{B}}_\mathbf{e}}\right)^\mathrm{D} - \rho_0 J^{-1}\int_0^\infty\left(2\bar{\mathbf{b}}_\mathbf{e}(\omega)\frac{\partial\tilde{\psi}_{fillers}}{\partial\bar{\mathbf{b}}_\mathbf{e}(\omega)}\right)^\mathrm{D} P(\omega)d\omega - \rho_0\left(\frac{\partial\psi_{vol}}{\partial J}\mathbf{1}\right)\right) : \mathbf{D} \\ &+ \left(2\rho_0 J^{-1}\bar{\mathbf{V}}_\mathbf{e}\frac{\partial\psi_{matrix}}{\partial\bar{\mathbf{B}}_\mathbf{e}}\bar{\mathbf{V}}_\mathbf{e} - 2\rho_0 J^{-1}\bar{\mathbf{V}}_\mathbf{e}^{-1}\overline{\mathbf{F}}_\mathbf{e}\bar{\mathbf{B}}_\mathbf{i}\frac{\partial\psi_{matrix}}{\partial\bar{\mathbf{B}}_\mathbf{i}}\overline{\mathbf{F}}_\mathbf{e}^{\,\mathrm{T}}\bar{\mathbf{V}}_\mathbf{e}^{-1}\right) : \bar{\mathbf{D}}_\mathbf{i}^\mathbf{o} \\ &+ 2\rho_0 J^{-1}\int_0^\infty\left(\bar{\mathbf{v}}_\mathbf{e}(\omega)\frac{\partial\psi_{fillers}}{\partial\bar{\mathbf{b}}_\mathbf{e}}\bar{\mathbf{v}}_\mathbf{e}(\omega)\right) : \bar{\mathbf{d}}_\mathbf{i}^\mathbf{o}(\omega)P(\omega)d\omega \geq 0 \end{aligned} \tag{11}$$

From equation (11), it is deduced the following constitutive equation for stress:

$$\boldsymbol{\sigma} = \overbrace{\left(2\rho_0 J^{-1}\bar{\mathbf{B}}_\mathbf{e}\frac{\partial\psi_{matrix}}{\partial\bar{\mathbf{B}}_\mathbf{e}}\right)^\mathrm{D}}^{\boldsymbol{\sigma}_{matrix}} + \overbrace{\int_0^\infty\underbrace{\left(2\rho_0 J^{-1}\bar{\mathbf{b}}_\mathbf{e}(\omega)\frac{\partial\tilde{\psi}_{fillers}}{\partial\bar{\mathbf{b}}_\mathbf{e}(\omega)}\right)^\mathrm{D}}_{\tilde{\boldsymbol{\sigma}}_{filler}(\omega)} P(\omega)d\omega}^{\boldsymbol{\sigma}_{fillers}} + \overbrace{\rho_0\frac{\partial\psi_{vol}}{\partial J}\mathbf{1}}^{\boldsymbol{\sigma}_{vol}} \tag{12}$$

It remains two part in the dissipation which are assumed to be independently positives. A quadratic pseudo-potential is chosen for the matrix:

$$\varphi_{matrix}(\bar{\mathbf{D}}^{\mathbf{o}}_{\mathbf{i}}) = \frac{\eta}{2}(\bar{\mathbf{D}}^{\mathbf{o}}_{\mathbf{i}} : \bar{\mathbf{D}}^{\mathbf{o}}_{\mathbf{i}}) \tag{13}$$

Where η is a viscosity parameter of the matrix. Therefore, using the concept of normality, the thermodynamical force that drives inelastic effects in the matrix is defined from the variation of the pseudo-potential. Assuming the isotropy of the free energy function, the first complementary equation is obtained:

$$\bar{\mathbf{D}}^{\mathbf{o}}_{\mathbf{i}} = \frac{2\rho_0}{J\eta}\left(\bar{\mathbf{B}}_{\mathbf{e}}\frac{\partial\psi_{matrix}}{\partial\bar{\mathbf{B}}_{\mathbf{e}}} - 2\bar{\mathbf{V}}^{-1}_{\mathbf{e}}\left(\psi_{matrix,1}\bar{\mathbf{B}} - \psi_{matrix,2}\bar{\mathbf{B}}_{\mathbf{e}}\bar{\mathbf{B}}^{-1}\bar{\mathbf{B}}_{\mathbf{e}}\right)\bar{\mathbf{V}}^{-1}_{\mathbf{e}}\right)^{\mathrm{D}} \tag{14}$$

In the previous equation, $\psi_{matrix,1}$ and $\psi_{matrix,2}$ stands for the variations of the isotropic free energy upon the inelastic invariants:

$$\psi_{matrix,1} = \frac{\partial\psi_{matrix}}{\partial I_1(\bar{\mathbf{B}}_{\mathbf{i}})} \qquad \psi_{matrix,2} = \frac{\partial\psi_{matrix}}{\partial I_2(\bar{\mathbf{B}}_{\mathbf{i}})} \tag{15}$$

Concerning the second part in the residue of dissipation, as $P(\omega)$ is a positive function the following condition is sufficient to fulfill the Clausius-Duhem inequality:

$$\left(\bar{\mathbf{v}}_{\mathbf{e}}(\omega)\frac{\partial\psi_{fillers}}{\partial\bar{\mathbf{b}}_{\mathbf{e}}}\bar{\mathbf{v}}_{\mathbf{e}}(\omega)\right) : \bar{\mathbf{d}}^{\mathbf{o}}_{\mathbf{i}}(\omega) \geq 0 \qquad \forall\omega \in [0,\infty[\tag{16}$$

We define an elastic domain:

$$\mathbb{E}(\omega) = \{\tilde{\boldsymbol{\sigma}}_{filler} | f(\tilde{\boldsymbol{\sigma}}_{filler},\omega) \leq 0\} \tag{17}$$

where f is a yield stress function for which the yield depends on ω. We assume the following form for the dual[2] pseudo-potential of dissipation:

$$\varphi^* = \frac{\langle f(\tilde{\boldsymbol{\sigma}}_{filler},\omega)\rangle^2}{2\beta(\omega)} \qquad \text{with} \qquad f(\tilde{\boldsymbol{\sigma}}_{filler},\omega) = \|\tilde{\boldsymbol{\sigma}}_{filler}\| - \chi(\omega) \tag{18}$$

where $\beta(\omega)$ is a viscosity function, $< . >$ are the Mac-Cauley brackets[3], $\chi(\omega)$ is the yield parameter. Using the normality principle, we obtain the following expression:

$$\bar{\mathbf{d}}^{\mathbf{o}}_{\mathbf{i}}(\omega) = \frac{\partial\varphi^*}{\partial\tilde{\boldsymbol{\sigma}}_{filler}} = \frac{\langle f(\tilde{\boldsymbol{\sigma}}_{filler})\rangle}{\beta(\omega)}\frac{\tilde{\boldsymbol{\sigma}}_{filler}}{\|\tilde{\boldsymbol{\sigma}}_{filler}\|} \tag{19}$$

To proceed further, we make the following choices for the free energies:

$$\begin{cases} \rho_0\psi_{matrix} = C_1\left(I_1(\bar{\mathbf{B}}_{\mathbf{e}}) - 3\right) + C_2\ Ln\left(\dfrac{I_2(\bar{\mathbf{B}}_{\mathbf{e}})}{3}\right) + A\left(I_1(\bar{\mathbf{B}}_{\mathbf{i}}) - 3\right) \\ \rho_0\tilde{\psi}_{fillers}\left(\omega, \bar{\mathbf{b}}_{\mathbf{e}}(\omega)\right) = a(\omega)\left(I_1(\bar{\mathbf{b}}_{\mathbf{e}}(\omega)) - 3\right) \end{cases} \tag{20}$$

where C_1, C_2, A are material parameters. Concerning the statistical functions, we choose a Gaussian form for the density of probability, a linear form for the yield parameter and the viscosity of the fillers, the shear modulus of the fillers follows an exponential decay:

$$\begin{cases} P(\omega) = \dfrac{1}{P_0}\exp(-(\dfrac{\omega}{\Omega})^2) \\ \text{with } P_0 = \displaystyle\int_0^\infty \exp\Big[-\big(\frac{\omega}{\Omega}\big)^2\Big]d\omega \\ \chi(\omega) = \bar{\chi}\frac{\omega}{\omega_0}\ ,\ a(\omega) = a_0\exp\big(-\frac{\omega}{\omega_0}\big)\ ,\ \beta(\omega) = \bar{\beta}\frac{\omega}{\omega_0} \end{cases} \tag{21}$$

[2]Dual pseudo-potential (which depend on force) can be obtained from a Legendre-Fenchel transformation of the primal pseudo-potential (which depend on flux)

[3]Operator $< . >$ is defined by $< f >= (f + |f|)/2$

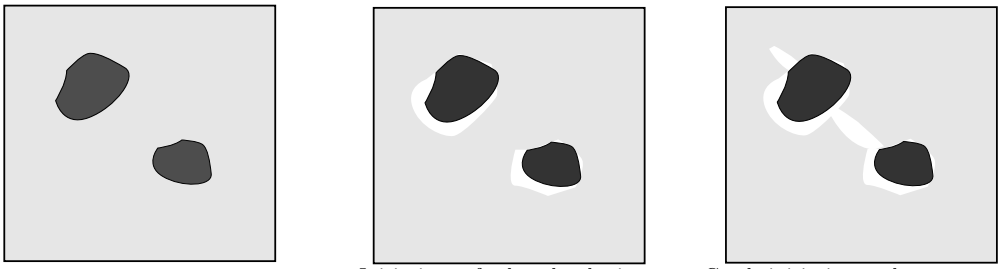

Virgin state

Initiation of the decohesion mechanism at the filler-matrix interface (described by d)

Crack initiation and propagation in the matrix (described by D)

Figure 8: Supposed damage senario

To resume, the constitutive model is defined from the following set of constitutive equations and flow rules:

$$\boxed{\begin{aligned}
&\boldsymbol{\sigma} = \boldsymbol{\sigma}_{matrix} + \int_0^\infty \tilde{\boldsymbol{\sigma}}_{filler} P(\omega) d\omega + p\mathbf{1} \\
&\boldsymbol{\sigma}_{matrix} = 2J^{-1}\left(C_1\bar{\mathbf{B}}_\mathbf{e} + \frac{C_2}{I_2(\bar{\mathbf{B}}_\mathbf{e})}(I_1(\bar{\mathbf{B}}_\mathbf{e})\mathbf{1} - \bar{\mathbf{B}}_\mathbf{e})\right)^{\mathrm{D}} \\
&\tilde{\boldsymbol{\sigma}}_{filler} = 2J^{-1}a(\omega)\bar{\mathbf{b}}_\mathbf{e}(\omega)^{\mathrm{D}} \\
&p = \rho_0 \frac{\partial \psi_{vol}}{\partial J} \\
&\dot{\bar{\mathbf{B}}}_\mathbf{e} = \mathbf{L}\bar{\mathbf{B}}_\mathbf{e} + \bar{\mathbf{B}}_\mathbf{e}\mathbf{L}^{\mathrm{T}} - \frac{2}{3}(\mathbf{1}:\mathbf{L})\bar{\mathbf{B}}_\mathbf{e} - \frac{2}{\eta}\,\boldsymbol{\sigma}_{matrix}\bar{\mathbf{B}}_\mathbf{e} + \frac{4A}{J\eta}\left(\bar{\mathbf{B}} - \frac{1}{3}(\bar{\mathbf{B}}:\bar{\mathbf{B}}_\mathbf{e}^{-1})\bar{\mathbf{B}}_\mathbf{e}\right) \\
&\dot{\bar{\mathbf{b}}}_\mathbf{e}(\omega) = \mathbf{L}\bar{\mathbf{b}}_\mathbf{e}(\omega) + \bar{\mathbf{b}}_\mathbf{e}(\omega)\mathbf{L}^{\mathrm{T}} - \frac{2}{3}(\mathbf{1}:\mathbf{L})\bar{\mathbf{b}}_\mathbf{e}(\omega) - 2\frac{\langle f(\tilde{\boldsymbol{\sigma}}_{filler})\rangle}{\beta(\omega)}\frac{\tilde{\boldsymbol{\sigma}}_{filler}}{\|\tilde{\boldsymbol{\sigma}}_{filler}\|}\bar{\mathbf{b}}_\mathbf{e}(\omega)
\end{aligned}} \tag{22}$$

There are **9** material parameters to identify, **7** are deterministic (C_1, C_2, A, η, a_0, $\bar{\beta}$ and $\bar{\chi}$) and **2** are statistical (Ω and ω_0).

3.2. Continuum fatigue damage model

We start from the following hypothesis: (1) the damage is isotropic, (2) the damage is accumulated in a linear manner and (3) the damage is composed by two contributions: *(i)* a microscopic one, that corresponds to the fillers/matrix de-cohesion observed with the SEM and *(ii)* a macroscopic one which is activated upon reaching a yield damage that corresponds to cracks propagation in the matrix leading to a stiffness loss.

In the constitutive model the statistical parameter Ω controls the probability to activate a micro-mechanism of dissipation in the aggregates. A larger value of Ω leads to a larger standard deviation. Therefore when matrix/fillers decohesion occurs the stress contribution of agglomerates decreases which can be represented by a smaller standard deviation. The micro damage d is then defined from the following relation:

$$\Omega = (1-d)\tilde{\Omega} \tag{23}$$

where $\tilde{\Omega}$ is the parameter of a virgin material. The macro damage D which concern only the matrix is classically defined from:

$$\boldsymbol{\sigma}_{matrix} = (1-D)\tilde{\boldsymbol{\sigma}}_{matrix} \tag{24}$$

where $\tilde{\boldsymbol{\sigma}}_{matrix}$ is the effective stress (which correspond to a virgin material). The figure 8 shows a schematic representation of the supposed damage scenario.

The internal variable rates $\dot{d}$ and $\dot{D}$ can be derived from a pseudo-potential of dissipation defined from the thermodynamical forces associated to damage, however in the following we consider the damage increment

over one cycle such as:

$$\frac{\delta d}{\delta N} = \int_{cycle} \dot{d} dt \qquad \text{and} \qquad \frac{\delta D}{\delta N} = \int_{cycle} \dot{D} dt \tag{25}$$

In this approach we postulate that the accumulation of damage is related to the difference between the power of internal forces and the dissipated energy integrated over a cycle. This energetic quantity is referred as a returnable cyclic energy. We define R_{matrix} and $R_{fillers}$, respectively the returnable cyclic energy of matrix and agglomerates such as:

$$\begin{cases} R_{matrix} = \displaystyle\int_{cycle} \left\langle \rho \dot{\psi}_{matrix} \right\rangle dt = \int_{cycle} \left\langle \boldsymbol{\sigma}_{matrix} : \mathbf{D} - \phi_{matrix} \right\rangle dt \\ R_{fillers} = \displaystyle\int_0^\infty \left(\int_{cycle} \left\langle \rho \dot{\tilde{\psi}}_{fillers}(\omega) \right\rangle dt \right) \mathcal{P}(\omega) d\omega = \int_{cycle} \left\langle \boldsymbol{\sigma}_{fillers} : \mathbf{D} - \phi_{fillers} \right\rangle dt \end{cases} \tag{26}$$

where $< x >$ denotes the positive part of x. Starting from these energies, we state a power law evolution for the micro damage over a cycle:

$$\frac{\delta d}{\delta N} = \frac{d^\alpha}{1-\alpha} \left(\frac{R_{fillers}}{R^0_{fillers}} \right)^\beta \quad \text{with} \quad \alpha < 1 \tag{27}$$

where α, β and $R^0_{fillers}$ are material parameters. For the macro damage over a cycle we also assume a power law evolution but with a yield function depending on the level of micro-damage. Therefore, we assume that a macro damage could not initiate if a micro-damage do not have reached the yield limit d_0:

$$\frac{\delta D}{\delta N} = \mathcal{H}(d - d_0) \frac{D^\zeta}{1-\zeta} \left(\frac{R_{matrix}}{R^0_{matrix}} \right)^\nu \quad \text{with} \quad \zeta < 1 \tag{28}$$

with $\mathcal{H}(x)$ a Heaviside function and ζ, ν, d_0, R^0_{matrix} material parameters. The integration of the equation (27) and (28) over cycles leads to the following:

$$d = \left(N \left(\frac{R_{fillers}}{R^0_{fillers}} \right)^\beta \right)^{\frac{1}{1-\alpha}} \tag{29}$$

$$D = \mathcal{H}(d - d_0) \left(N \left(\frac{R_{matrix}}{R^0_{matrix}} \right)^\nu \right)^{\frac{1}{1-\zeta}} \tag{30}$$

From the previous equations, it can be computed two maximum number of cycles N^{micro}_{limit} and N^{macro}_{limit}, which are defined from $d = 1$ and $D = 1$:

$$\begin{cases} N^{micro}_{limit} = \left(\dfrac{R_{fillers}}{R^0_{fillers}} \right)^{-\beta} & \\ N^{macro}_{limit} = \left(\dfrac{R_{matrix}}{R^0_{matrix}} \right)^{-\nu} & \text{if} \quad N^{macro}_{limit} > d_0^{1-\alpha} \left(\dfrac{R_{fillers}}{R^0_{fillers}} \right)^{-\beta} \\ N^{macro}_{limit} = \infty & \text{otherwise} \end{cases} \tag{31}$$

The end of life is reached when $D = 1$ which corresponds to the occurence of a macro crack in the matrix. The propagation of these macro cracks must be described by fracture mechanics and are not considered in this paper.

4. Parameters identification

4.1. Undamaged behavior

We use the same strategy as proposed in Martinez et al. (2011). This strategy consists in three steps: (1) Quasi-static experimental tests (tension and simple shear) allow to determine C_1, C_2 and to estimate A, a_0, $\bar{\chi}$, Ω and ω_0; (2) Relaxation tests (tension and simple shear) allow to identify A, H and ω_0, and to correct a_0, $\bar{\chi}$, $\bar{\eta}$, Ω and (3) triangular cyclic tests, at different rates (simple shear) allow to correct the prediction of a_0, $\bar{\chi}$, $\bar{\eta}$ and Ω.

Each step of identification is realized with an heuristic algorithm of minimization of the sum of the squared distances between the experimental data and the analytical or semi-analytical responses. The material parameters obtained are presented in table 2.

Figures 9 show the responses of the identified model compared to experimental tests. Some tests have been used in the identification strategy, this is the case for figures 9(a), 9(b) and 9(c). Others are used for validation purpose, this is the case of figure 9(d). Comparatively to the previous version of the statistical approach that has been presented in Martinez et al. (2011), the present model exhibits a better agreement to the experimental tests.

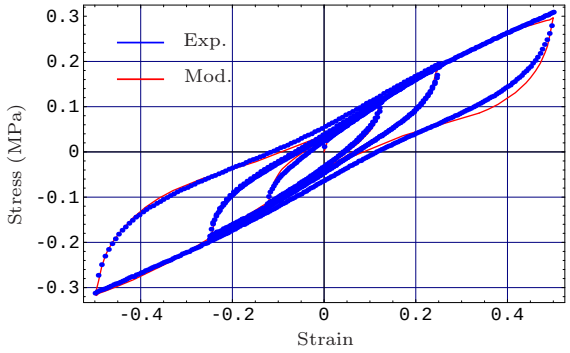

(a) Quasi-static triangular shear test: progressive amplitudes and fixed deformation rate

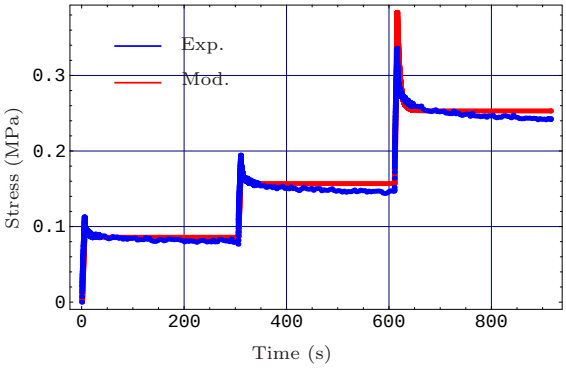

(b) Relaxation test in simple shear with a progressive amplitude

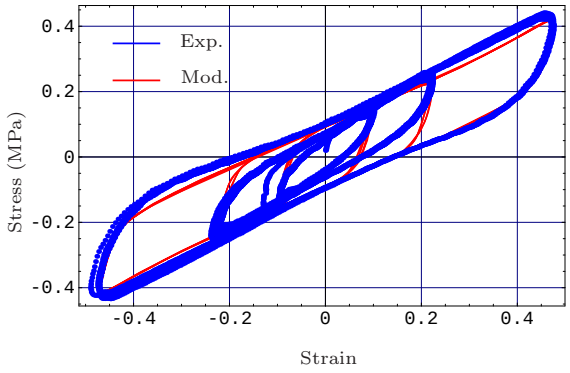

(c) Dynamic triangular shear test with progressive amplitudes ($\dot{\gamma} = 10s^{-1}$)

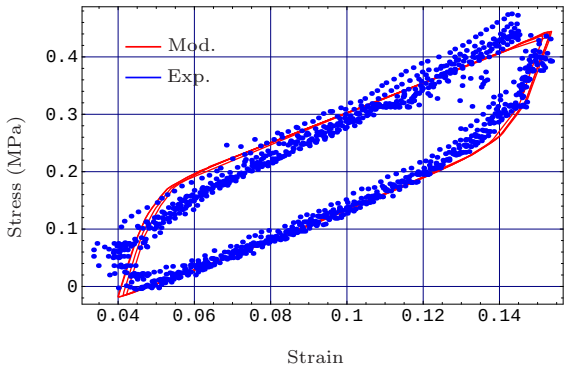

(d) Uni-axial triangular tension test ($\dot{\lambda} = 1s^{-1}$)

Figure 9: Comparison of the identified model and some experiments in shear and tension.

4.2. Damage parameters

To identify the damage parameters, only uni-axial tension tests are used because we assume that the central zone of the specimen sees a uniform damage which is clearly not the case of the simple shear specimen.

C_1	C_2	A	η	a_0	$\bar{\beta}$	$\bar{\chi}$	Ω	ω_0
1.28 Mpa	-2.67 Mpa	2.95 Mpa	50.13 Mpa.s	5.12 Mpa	0.5 Mpa.s	1.69 Mpa	$3.11e^{-2}$	0.40

Table 2: Material parameters

Therefore, for each fatigue test in tension it is identified a set of material parameters as explained in the previous section. Using the definition of eqs. (23) and (24), it is computed the value of d, D, R_{matrix} and $R_{fillers}$ for each configuration of fatigue. Taking logarithmic value of eqs. (27) and (28), one can separate the identification of α and A from the others parameters. Figures 10(a) and 11(a) show the evolution of the damage rate upon the current value of damage computed after each characterization test done after a fixed number of cycles (repeated for each configuration of fatigue). The parameters α and A can be identified from these curves. Figures 10(b) and 11(b) show the dependance of damage upon returnable cyclic energy. The parameters β, B, $R^0_{fillers}$ and R^0_{matrix} can be computed from these curves. The last parameter, d_0, is determined by computing a mean of d values for which D starts to increase. The parameters are given in table 3.

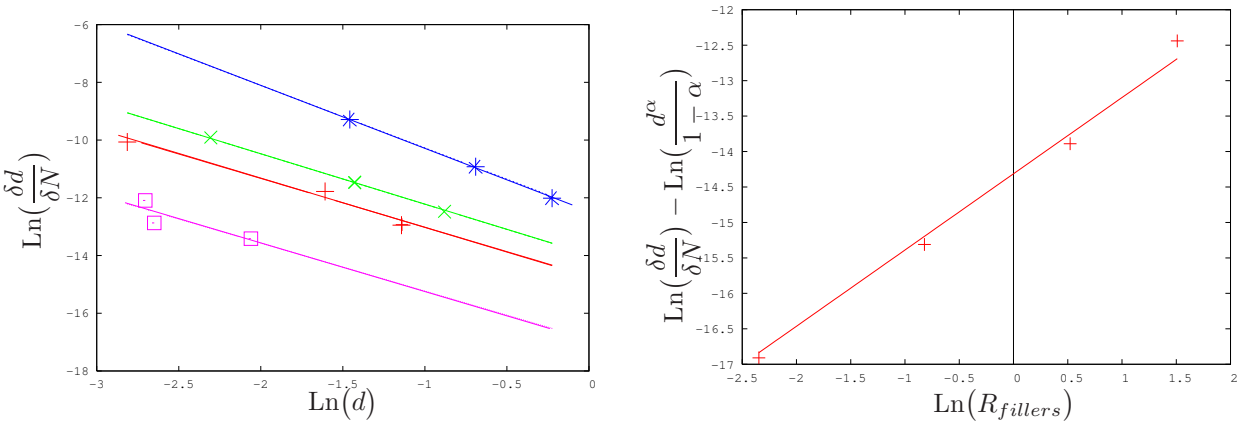

(a) Damage rate evolution for different fatigue tests at 0.5Hz (□ : 25±25% of strain, + : 50±50% of strain, × : 100±100% of strain, ✳ : after 150 ± 150% of strain).

(b) Residue of damage rate for the different fatigue configurations

Figure 10: Micro damage identification

α	ζ	β	ν	$R^0_{fillers}$	R^0_{matrix}	d_0
-1.84	-0.25	1.07	0.62	$2.81e^5$	$7.74e^8$	0.085

Table 3: Damage parameters

5. Finite elements simulations

5.1. Variational Formulation

To resolve the equilibrium equations in a quasi-static context with a nearly-incompressible constitutive behavior it has been chosen a perturbed Lagrangian weak form. This formulation is based on the introduction of a Lagrange multiplier, p which stands for the hydrostatic pressure. Therefore, the equilibrium solution is defined by the couple $(\boldsymbol{u}, p)$ which have to cancel the following integral form for all the test functions

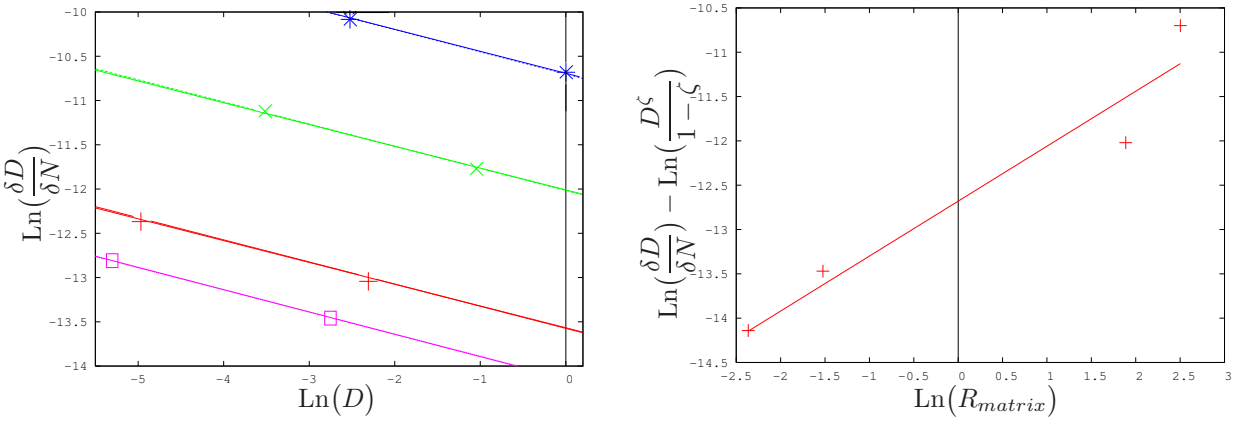

(a) Damage rate evolution for different fatigue configurations (□ : after ±25% of fatigue, + : after ±50% of fatigue, × : after ±100% of fatigue, ✳ : after ±150% of fatigue).

(b) Residue of damage rate for the different fatigue configurations

Figure 11: Macro damage identification

$(\delta \boldsymbol{u}, \delta p)$:

$$\begin{cases} \displaystyle\int_{\Omega_0} (\boldsymbol{\Pi}_{matrix} + \boldsymbol{\Pi}_{fillers} + pJ\mathbf{F}^{-\mathrm{T}}) : \nabla \delta \boldsymbol{u} d\Omega - \int_{\Omega_0} \delta \boldsymbol{u} \cdot \mathbf{f_{vol}} d\Omega - \int_{\delta\Omega_{0f}} \delta \boldsymbol{u} \cdot \mathbf{f_{surf}} dS = 0 \\ \displaystyle\int_{\Omega_0} \left(g(J) - \frac{p}{K} \right) \delta p d\Omega = 0 \end{cases} \tag{32}$$

where Ω_0 is the initial domain (in the reference configuration), $\delta\Omega_{0f}$ is the initial boundary where current surface forces $\mathbf{f_{surf}}$ are applied, $\mathbf{f_{vol}}$ are the current volumetric forces. Tensors $\boldsymbol{\Pi}_{matrix}$ and $\boldsymbol{\Pi}_{fillers}$ stand for the first Piola-Kirchof stress respectively in the matrix and in the fillers, they are defined from the following relations:

$$\boldsymbol{\Pi}_{matrix} = J\boldsymbol{\sigma}_{matrix}\mathbf{F}^{-\mathrm{T}} \qquad \text{and} \qquad \boldsymbol{\Pi}_{fillers} = J\boldsymbol{\sigma}_{fillers}\mathbf{F}^{-\mathrm{T}} \tag{33}$$

The parameter K is the compressibility modulus and its inverse plays a role of a perturbation parameter. The compressibility function $g(J)$, is defined from the following relation:

$$g(J) = \rho_0 \frac{1}{K} \frac{\partial \psi_{vol}}{\partial J} \tag{34}$$

in this paper, the classical linear compressibility law is used leading to the following free energy potential:

$$\rho_0 \psi_{vol} = \frac{K}{2}(J-1)^2 \tag{35}$$

5.2. Numerical Implementation

The integration of the constitutive model defined by eqs (22), requires to compute the statistical integral form and the integration of the local flow rules. The statistical integration is realized by a classical trapezoidal scheme such as:

$$\boldsymbol{\sigma}_{fillers} = \sum_{k=1}^{n-1} \frac{1}{2} \left(\tilde{\boldsymbol{\sigma}}_{fillers}(\omega_k) P(\omega_k) + \tilde{\boldsymbol{\sigma}}_{fillers}(\omega_{k+1}) P(\omega_{k+1}) \right) (\omega_{k+1} - \omega_k) \tag{36}$$

where ω_k is defined from the number of integration points n such as: $\omega_k = k(\omega_e)/n$, ω_e is an activation energy limit associated with a probability of $0.01P_0$:

$$\omega_e = \sqrt{-\ln(0.01)\Omega^2} \tag{37}$$

Therefore, the computation of $\boldsymbol{\sigma}_{fillers}$ requires the resolution of n flow rules. Each flow rule, is integrated with a specific backward Euler scheme which is detailed in Lejeunes et al. (2011). In practice, these computations are easy to parallelize as the flow rules are not dependent from each other. Therefore, it has been chosen the following strategy: at each gauss point the sum defined by eq. (36) is parallelized using an OpenMP framwork. Each cpu core solves a flow rule with its own copy of $\mathbf{b}_e(\omega)$. The computing time is directly related to the stiffness of the differential system of equations obtained for each flow rule. Therefore this strategy is not optimal but it is very easy to implement.
The computation of a local state of damage requires the evaluation of the returnable cyclic energy R_{matrix} and $R_{fillers}$, as for the statistical integration, a trapezoidal integration rule is used to compute the integrals of equation (26).
The space discretization is realized with classical stable mixed elements with a linear interpolation for the pressure and a quadratic one for the kinematic field.

5.3. Simulation of the simple shear test

As mentioned previously, the simple shear test leads to an inhomogeneous state of damage, therefore it is proposed to use the results of this test as a validation purpose. As mentioned previously, the shear specimens used in this work, exhibit a specific shape with a meniscus on each lateral faces to enforce an initiation of damage in rubber and not in the interface rubber/aluminum (see figure 12(a)). Experimentally it was observed a macroscopic crack initiation near the center of the meniscus which propagates with an approximate angle of 45^o. In some pathological tests the crack rapidly attains the aluminum layer and a decohesion of the aluminum/rubber interface is observed (see figure 12(b)).

For the finite elements simulation we assumed plane strain conditions, the aluminum is supposed to be perfectly rigid and not modelized. The mesh comprises 1183 nodes and 265 quadratic elements. To ensure that the numerical response corresponds to a stabilized response it is done five cycles of shear loading (transversal displacements with no vertical displacements are imposed on the top edge). The returnable cyclic energies are computed on the last cycle and the maximum number of cycles (lifetime) is deduced.

The figure 13 shows the evolution of the two damage variables, d and D in the shear specimen for a fatigue configuration of $\pm 50\%$ of shear strain at $6Hz$. It can be observed first that the maximum of macro damage is located near the center of the meniscus which is in good accordance to experimental observations. Furthermore, it can be also seen that the macro damage seems more inhomogeneous than the micro damage. Figure 14 shows a comparison of the global response of the numerical shear specimen and the experimental data. The stiffness loss seems well predicted by the model. It can also be computed a predicted life time (N^{macro}_{limit}) which is given by the minimum number of cycles for which $D = 1$ in a sufficiently large

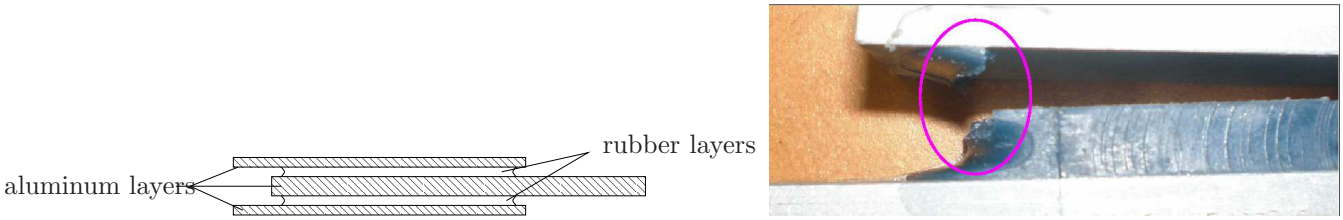

(a) Simple shear specimen with meniscus

(b) Decohesion of rubber/aluminum interface

Figure 12: Shear specimen

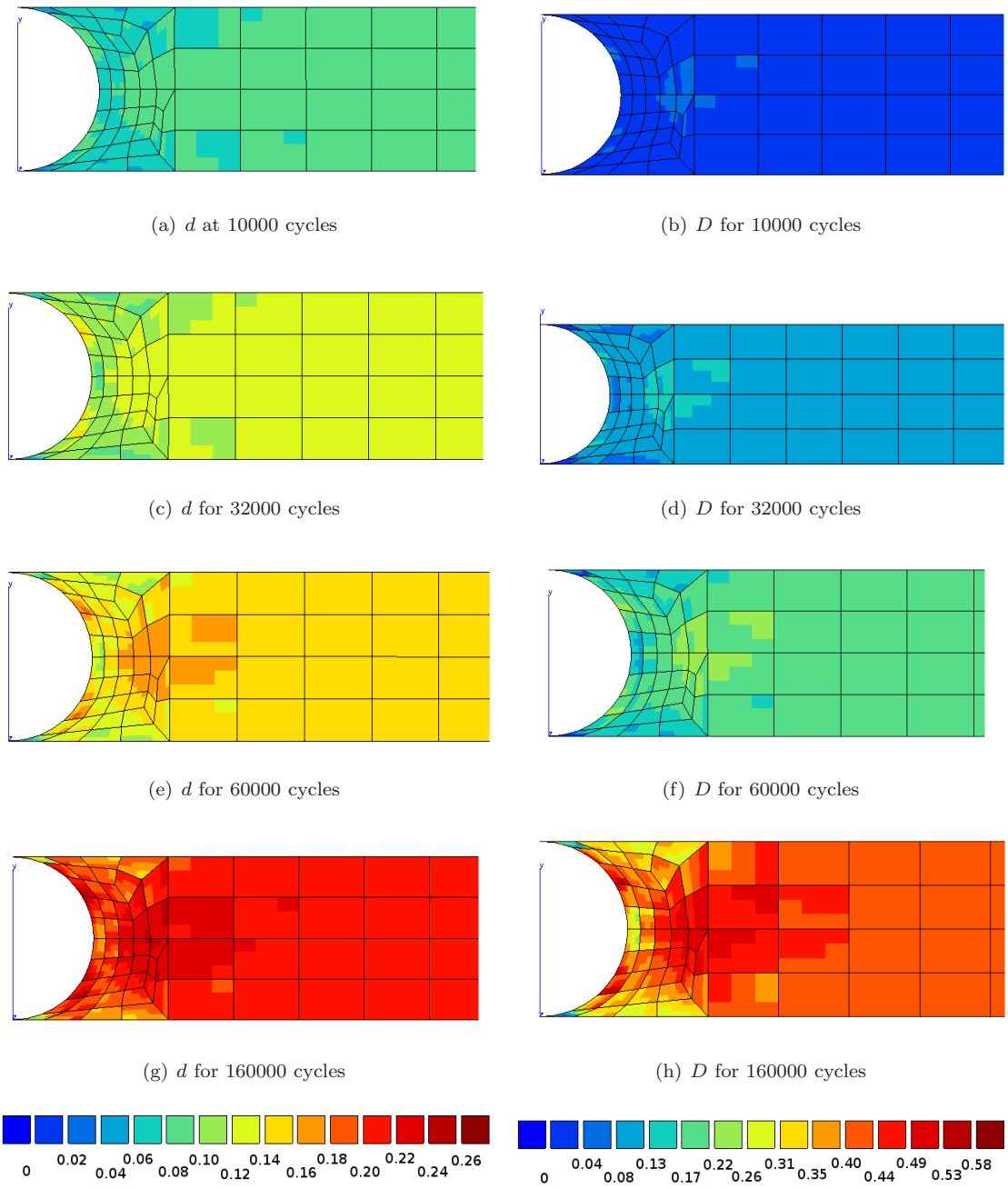

(a) d at 10000 cycles

(b) D for 10000 cycles

(c) d for 32000 cycles

(d) D for 32000 cycles

(e) d for 60000 cycles

(f) D for 60000 cycles

(g) d for 160000 cycles

(h) D for 160000 cycles

Figure 13: Evolution of the two damage fields for the shear specimen near the meniscus. Sinusoidal shear fatigue test at $\gamma = 0.5$ and $f = 6Hz$.

zone of the specimen (here it has been considered that 90% of the specimen area was a sufficiently large zone.). The table 4, presents some results of predicted life time for different fatigue configurations. As already seen experimentally it is observed a non linear dependence upon the solicitation amplitude and a weak influence of the frequency, at least in the experimental range. Unfortunately, these results cannot be confronted to experimental one as we do not have made enough tests in simple shear to be representative (the aluminum/rubber interface has broken suddenly in many tests).

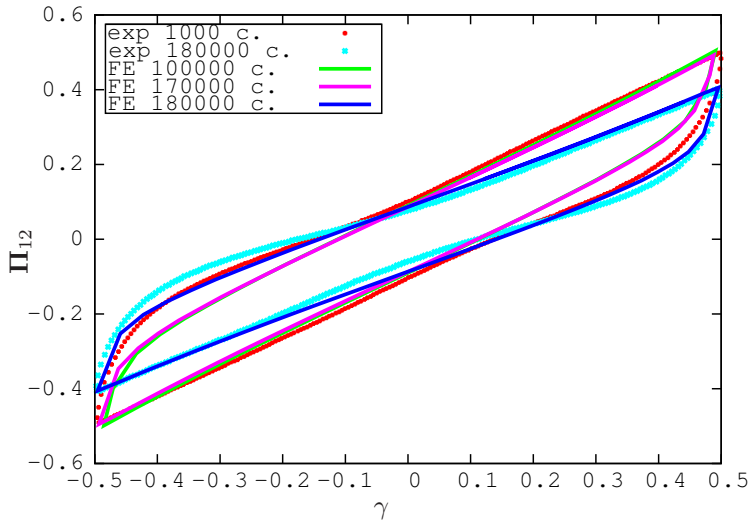

Figure 14: Evolution of the hysteresis upon the number of fatigue cycles for the shear specimen. Sinusoidal shear fatigue test at $\gamma = 0.5$ and $f = 6Hz$.

Frequency (Hz)	Shear amplitude (%)	N_{limit}^{macro} (number of cycles)
6	12.5	2044793
6	25	931663
6	50	400564
15	25	931779
15	50	401318

Table 4: Predicted life time ($D = 1$) for different fatigue configuration in simple shear

6. Concluding remarks

The use of continuum damage mechanics for rubber seems promising for at least two reasons. First, the experimental campaign for such an approach is less time consuming than approaches that are based on Whöler curves or Haigh's diagram. Furthermore, interlaying characterization tests in a fatigue test allows to separate thermal softening from damage softening. Second, the model is not restricted to only one damage mechanism or one physical criteria to predict the fatigue behavior. In the present paper, it has been considered two damage mechanisms which are micro-mechanically motivated: filler agglomerates decohesion and matrix voids or cracks growth. Therefore, these models can propose a link between micro-mechanical observations and fatigue behavior.

The silicon rubber that is considered in this paper exhibits a complex behavior. We have observed a thermal aging previously to damage softening. We assume that this effect is due to a chemical activity (cross-liking) during the fatigue test. However, a systematic chemo-physical characterization is needed to study this effect.

The proposed model is based on a micro-motivated approach with a statistical representation of agglomerates populations. It allows a continuous representation of the characteristic times of viscosity. Therefore, the introduction of a micro damage variable that affects fillers/matrix interface behavior is straight forward: only one statistical variable has to be considered. The main originality of this model resides in the introduction of the returnable cyclic energy to build damage evolution laws. This energy takes into account of dissipation and free energy. In this paper, it is only considered mechanical dissipation as thermal effects has been neglected. However, the proposed criteria can be extended to a thermo-mechanical case.

The finite element implementation of the proposed model has allowed to confront some numerical results in simple shear to experimental ones for a model which has been identified in tension. First results are

encouraging but more experimental tests have to be done. In a future work, we will looking at diabolo specimens to do tension/torsion or compression/torsion tests.

References

Andriyana, A., Saintier, N., Verron, E., 2010. Configurational mechanics and critical plane approach: Concept and application to fatigue failure analysis of rubberlike materials. International Journal of Fatigue 24, 949–961.

Ayoub, G., Nat-Abdelaziz, M., Zari, F., Gloaguen, J., Charrier, P., 2011. A continuum damage model for the high-cycle fatigue life prediction of styrene-butadiene rubber under multiaxial loading. International Journal of Solids and Structures 48 (18), 2458 – 2466.
URL http://www.sciencedirect.com/science/article/pii/S0020768311001405

Ayoub, G., Nat-Abdelaziz, M., Zari, F., Gloaguen, J., Charrier, P., 2012. Fatigue life prediction of rubber-like materials under multiaxial loading using a continuum damage mechanics approach: Effects of two-blocks loading and r ratio. Mechanics of Materials 52 (0), 87 – 102.
URL http://www.sciencedirect.com/science/article/pii/S0167663612000701

Beatty, J., 1964. Fatigue of rubber. Rubber Chemistry and Technology 37, 1341–1364.

Brunac, J., Gérardin, O., Leblond, J., 2009. On the heuristic extension of haigh's diagram for the fatigue of elastomers to arbitrary loadings. International Journal of Fatigue 31, 850–867.

Cadwell, S., Merrill, R., Sloman, C., 1940. Dynamic fatigue life of rubber. Industrial and Engineering Chemistry, Analytical Edition 12, 19–23.

Chagnon, G., Verron, E., Gornet, L., Marckmann, G., Charrier, P., 2004. On the relevance of continuum damage mechanics as applied to the mullins effect in elastomers. Journal of the Mechanics and Physics of Solids 52 (7), 1627 – 1650.
URL http://www.sciencedirect.com/science/article/pii/S002250960400002X

Flory, R. J., 1961. Thermodynamic relations for highly elastic materials. Transactions of the Faraday Society 57, 829–838.

Lacroix, F., Méo, S., Berton, G., Chalon, F., Tougui, A., Ranganathan, N., 2005. A local criterion for fatigue crack initiation on chloroprene rubber: approach in dissipation. In: Constitutive models for rubber IV.

Lake, J., Lindley, P., 1965. The mechanical fatigue limit for rubber. Journal of Applied Polymer Science 9, 1233–1251.

Legorju-jago, K., Bathias, C., 2002. Fatigue initiation and propagation in natural and synthtic rubbers. International Journal of Fatigue vol. 24, p. 85–92.

Lejeunes, S., Boukamel, A., Méo, S., 2011. Finite element implementation of nearly-incompressible rheological models based on multiplicative decomposition. Computers and Structures 89, 411–421.

Lemaitre, J., 1985. A continuous damage mechanics model for ductile fracture. Journal of Engineering Material Technology 107, 83–89.

Mars, W., 2001. Multiaxial fatigue of rubber. Ph.D. thesis, University of Toledo.

Mars, W., 2002. Cracking energy density as a predictor of fatigue life under multiaxial conditions. Rubber Chemistry and Technology 75, 1–17.

Mars, W., Fatemi, A., 2002. A literature survey on fatigue analysis approaches for rubber. International Journal of Fatigue 24, 949–961.

Martinez, J., Boukamel, A., Méo, S., Lejeunes, S., 2011. Statistical approach for a hyper-visco-plastic model for filled rubber: Experimental characterization and numerical modeling. European Journal of Mechnics A/Solids 30, 1028–1039.

Poisson, J., Lacroix, F., Méo, S., Berton, G., Ranganathan, N., 2011. Biaxial fatigue behavior of a polychloroprene rubber. International Journal of Fatigue 33, 1151–1157.

Previati, G., Kaliske, M., 2012. Crack propagations in pneumatic tires: Continuum mechanics and fracture mechanics approaches. International Journal of Fatigue 37.

Robisson, A., Avril 2000. Comportement d'un élastomère sbr chargé de silice et d'un pu cellulaire: Prévision de la durée de vie en fatigue. Ph.D. thesis, Ecole des Mines de Paris.

Saintier, N., Cailletaud, G., Piques, R., 2006. Crack initiation and propagation under multiaxial fatigue in a natural rubber. International Journal of Fatigue 28, p. 61–72.

Saintier, N., Cailletaud, G., Piques, R., 2011. Cyclic loadings and crystallization of natural rubber: An explanation of fatigue crack propagation reinforcement under a positive loading ratio. Materials Science and Engineering: A 528, p. 1078–1086.

Verron, E., Andriyana, A., 2008. Definition of a new predictor for multiaxial fatigue crack nucleation in rubber. Journal of the Mechanics and Physics of Solids 56.

Verron, E., Le Cam, J., Gornet, L., 2005. A multiaxial criterion for crack nucleation in rubber. Mechanics Research Communications 33, 493–498.

Wang, B., Lu, H., ho Kim, G., 2002. A damage model for the fatigue life of elastomeric materials. Mechanics of Materials 34 (8), 475 – 483.
URL http://www.sciencedirect.com/science/article/pii/S0167663602001758

Zine, A., Benseddiq, N., Abdelaziz, M., 2011. Rubber fatigue life under multiaxial loading: Numerical and experimental investigations. International Journal of Fatigue 33, 1360–1368.